

# Nonlinear Controllers for Wing Morphing Trajectories of a Heave Dynamics Model

Animesh Chakravarthy, Katie A. Evans, Johnny Evers, and Lisa M. Kuhn

**Abstract**—A multiple component structure consisting of two Euler-Bernoulli beams connected to a rigid mass is used to model the heave dynamics of an aeroelastic wing micro air vehicle that is acted upon by a nonlinear aerodynamic lift force. In this work we consider two different strategies for designing nonlinear controllers that achieve specified wing morphing trajectories, namely (a) linearization followed by linear quadratic tracking and (b) a feedback linearization inner loop with sliding mode outer loop. We seek to analyze the relative performance of the two controllers as we note the advantages and disadvantages of each approach.

## I. INTRODUCTION

The motivation for this work stems from interest in the development of flexible-wing micro aerial vehicles (MAVs). In recent years, much research has been stimulated by the notion of biologically-inspired flight, including aerodynamics, structural dynamics, flight mechanics, and control (see, for example, [1],[2],[3], and [4]). Traditional controllers designed using methods applicable to fixed wing aircraft are unlikely to realize the agile flight potential of flexible wing MAV airframes. While there are projects underway which involve control studies of biological flight, it is our goal to examine vehicular modeling as a whole while simultaneously seeking to exploit the model for control design.

An initial model representing the heave dynamics of a flexible wing MAV was presented in [5]. The model was elaborated upon and its ability to track to a desired state was tested in [6]. In this work we employ two approaches for obtaining morphing wing trajectories over time: feedback linearization inner loop with a sliding mode controller and linear quadratic tracking control. We seek to analyze the controllers' performance via morphing trajectory over time, and note advantages and disadvantages of each approach.

This work was supported by NSF EPSCoR through the Louisiana Board of Regents under Contract Number NSF(2010)-PFUND-201, the US Air Force Summer Faculty Fellowship Program, and the Air Force Research Laboratory under Contract Number FA8651-08-D-0108.

A. Chakravarthy is with the Faculty of Aerospace Engineering and Electrical Engineering, Wichita State University, 1845 N. Fairmount, Wichita, KS 67260, USA [animesh.chakravarthy@wichita.edu](mailto:animesh.chakravarthy@wichita.edu)

K. Evans is with the Faculty of Mathematics and Statistics, P.O. Box 10348, Louisiana Tech University, Ruston, LA 71272, USA [kevans@latech.edu](mailto:kevans@latech.edu)

J. Evers is with the Air Force Research Laboratory, Munitions Directorate, 101 W. Eglin Blvd., Ste. 332, Eglin AFB, FL 32542 USA [johnny.evers@eglin.af.mil](mailto:johnny.evers@eglin.af.mil)

L. Kuhn is with the Faculty of Mathematics, SLU Box 13057, Southeastern Louisiana University, Hammond, LA 70402, USA [lisa.kuhn@selu.edu](mailto:lisa.kuhn@selu.edu)

## II. CONTROL TECHNIQUES

### A. Feedback Linearization

While there does not appear to be controller existence results for the feedback linearization scheme for general nonlinear PDE systems, there is an existence result for hyperbolic quasi-linear systems [7]. Further, even in the absence of such existence or convergence guarantees, others have used feedback linearization and backstepping with success for control design on nonlinear PDE systems (see, for example, [8], [9], [10], [11], [12]). Thus, a feedback linearization approach appears to be a reasonable option to explore for this problem. In light of the lack of feedback linearization theoretical results in the infinite-dimensional setting, the following discussion is posed in finite dimensions.

Consider a nonlinear multi-input multi-output system that is input-affine of the form:

$$\dot{x} = f(x(t)) + \sum_{k=1}^m g_k(x(t))u_k(t) \quad (1)$$

$$y_i = h_i(x(t)); i = 1, 2, \dots, m \quad (2)$$

It is desired to develop a linear relationship between the output vector  $h(x)$  and a synthetic input vector  $V(t)$ . In order to achieve this, each of the output channels  $y_i$  is successively differentiated, until a coefficient of a control is non-zero [13]. Using Lie derivative notation, we get

$$\frac{d^{r_i} y_i}{dt^{r_i}} = L_f^{r_i}(h_i(x)) + \sum_{k=1}^m \langle dL_f^{r_i-1}(h_i(x)), g_k \rangle u_k \quad (3)$$

If the nonlinear system is input-output linearizable, then for each output  $y_i$ , a relative degree (also called linearizability index)  $r_i$  exists such that

$$\begin{aligned} \langle dL_f^m(h_i(x)), g_k \rangle &= 0, \quad \text{for } m = 1, 2, \dots, r_i - 1 \\ &\neq 0, \quad \text{for } m = r_i \end{aligned} \quad (4)$$

Then we can write the synthetic input vector  $V(t)$  in the form

$$V(t) = L(x(t)) + J(x(t))u(t) \quad (5)$$

where

$$L(x) = \begin{bmatrix} L_f^{r_1}(h_1(x)) \\ L_f^{r_2}(h_2(x)) \\ \dots \\ L_f^{r_m}(h_m(x)) \end{bmatrix} \quad (6)$$

and

$$J(x) = \begin{bmatrix} \langle dL_f^{r_1-1}(h_1(x)), g_1 \rangle & \cdots & \langle dL_f^{r_1-1}(h_1(x)), g_m \rangle \\ \langle dL_f^{r_2-1}(h_2(x)), g_1 \rangle & \cdots & \langle dL_f^{r_2-1}(h_2(x)), g_m \rangle \\ \cdots & \cdots & \cdots \\ \langle dL_f^{r_m-1}(h_m(x)), g_1 \rangle & \cdots & \langle dL_f^{r_m-1}(h_m(x)), g_m \rangle \end{bmatrix}. \quad (7)$$

An outer-loop controller is then constructed for the above feedback-linearized system. Define  $Y_d(t)$  as the desired output vector, i.e.

$$Y_d(t) = [ Y_{d1}(t) \quad Y_{d2}(t) \quad \cdots \quad Y_{dm}(t) ]^T \quad (8)$$

where  $Y_{di}(t)$  represents the desired output trajectory for the  $i$ <sup>th</sup> output. Then a set of surfaces,  $S$ , representing the desired dynamics of the errors between the values of the true and the desired outputs, is defined for the outer loop sliding controller. Thus  $S_i$  is the  $i$ <sup>th</sup> element of  $S$  and is a function of the derivative of  $y_i$  up to the  $(r_i - 1)$ <sup>th</sup> order.

$$S_i = \sum_{k=1}^{r_i-1} \beta_{ik} \frac{d^k(y_i - y_{di})}{dt^k} \quad (9)$$

$$\dot{S} = Y_d - L(x) - J(x)u \quad (10)$$

Taking  $F(s) = [F_1(s) \quad F_2(s) \quad \cdots \quad F_m(s)]^T$ , with  $F_i(s) = \eta_i \operatorname{sgn}(S_i)$  and  $\eta_i > 0$ , we can satisfy  $\dot{S}_i S_i < 0$  for all  $i = 1, 2, \dots, m$ . The control law is eventually obtained as

$$u = J(x)^{-1}[Y_d - L(x) + F(s)] \quad (11)$$

The existence of  $J(x)^{-1}$  is related with conditions involving the output controllability and the invertibility matrices [13].

### B. Linear Quadratic Tracking

Here we consider two cases of the standard Linear Quadratic Tracking problem. It is important to note that we pose the following discussion in an infinite dimensional setting since theory is in place to guarantee convergence of finite dimensional approximations to the PDE controller under usual assumptions (see [14] and [15]). We first consider the case where full state knowledge is assumed, more commonly known as Linear Quadratic Regulator (LQR) state tracking design, where the tracking problem reduces to a disturbance-rejection problem of the form

$$\dot{x}(t) = \mathcal{A}x(t) + \mathcal{B}u(t) + w(t), \quad x(0) = x_0, \quad (12)$$

where  $x(t) = x(t, \cdot) = \xi(t, \cdot) - \tilde{\xi}(t, \cdot) \in X$ , a Hilbert space,  $w(t)$  is represented by

$$w(t) = \mathcal{A}\tilde{\xi} - \dot{\tilde{\xi}} \neq 0, \quad (13)$$

$\xi$  is the state of some original dynamical linear system of interest,

$$\dot{\xi}(t) = \mathcal{A}_0\xi(t) + \mathcal{B}_0u(t) + z, \quad \xi(0) = \xi_0, \quad (14)$$

$\tilde{\xi}$  is the known desired state target of (14), and  $z$  is zero-mean, Gaussian, white noise. Here,  $\mathcal{A}$  is the linearized system operator defined on  $\mathbf{D}(\mathcal{A}) \subseteq X$  that, by assumption, generates a  $C_0$ -semigroup,  $\mathcal{B}$  is the control operator, and  $u(t)$  is the

control input, defined on a Hilbert space  $U$ , which is taken to be  $\mathbb{R}^m$  in this work.

The solution to the steady state tracking problem involves solving the standard control Riccati equation

$$\mathcal{A}^*\Pi + \Pi\mathcal{A} - \Pi\mathcal{B}R^{-1}\mathcal{B}^*\Pi + Q = 0 \quad (15)$$

for  $\Pi$ , where  $Q : X \rightarrow X$  is a state weighting operator, taken to be  $\mathcal{C}^*\mathcal{C}$  in this work (see (20)) and  $R : U \rightarrow U$  is a control weighting operator taken to be of the form  $R = cI$ , with  $c$  a scalar and  $I$  the identity operator, with both operators corresponding to the standard LQR cost function. Then the feedback control gain is defined as

$$\mathcal{K} = R^{-1}\mathcal{B}^*\Pi. \quad (16)$$

The feed forward signal  $u_{fw}$  is

$$u_{fw} = R^{-1}\mathcal{B}^*q, \quad (17)$$

where an approximation of  $q$  can be calculated by integrating backwards in time to obtain the steady state solution of

$$\dot{q}(t) = -[\mathcal{A} - \mathcal{B}R^{-1}\mathcal{B}^*\Pi]q(t), \quad (18)$$

with  $q(\infty) = 0$ , as stated in [16]. Then the control law for the LQR state tracking is

$$u(t) = -\mathcal{K}x(t) - u_{fw}, \quad (19)$$

which is implemented in (12).

The second Linear Quadratic control implementation involves an  $\mathcal{H}^2$ , specifically a Linear Quadratic Gaussian (LQG), state tracking design, where it is assumed that an estimate of the state from (12) exists, based on a measurement

$$y = \mathcal{C}x(t) + v, \quad (20)$$

where measurement  $y(t) : X \rightarrow Y$ , with  $Y$  a Hilbert space, is taken to be  $\mathbb{R}^p$  in this work,  $v$  is zero-mean, Gaussian, white noise, uncorrelated with  $z$  in (14), and the estimate,  $x_c(t) = x_c(t, \cdot) \in X$ , is used in the control law (19). Again, the state from (12) is  $\xi - \tilde{\xi}$ . It is assumed that the desired target of the state estimate is also  $\tilde{\xi}$ . To provide this estimate, a compensator is used that has the form

$$\dot{x}_c(t) = \mathcal{A}_c x_c(t) + \mathcal{F}_c y(t), \quad x_c(0) = x_{c0} \quad (21)$$

and the feedback control law is written

$$u(t) = -\mathcal{K}x_c(t) - u_{fw}, \quad (22)$$

where  $\mathcal{K}$  and  $u_{fw}$  are determined from the LQR tracking solution. From standard theory, it is well-known that by solving an additional filter Riccati equation

$$\mathcal{A}P + P\mathcal{A}^* - P\mathcal{C}^*\mathcal{C}P + \mathcal{B}\mathcal{B}^* = 0, \quad (23)$$

one can obtain the operators  $\mathcal{F}_c$ , and  $\mathcal{A}_c$  via

$$\begin{aligned} \mathcal{F}_c &= P\mathcal{C}^*, \\ \mathcal{A}_c &= \mathcal{A} - \mathcal{B}\mathcal{K} - \mathcal{F}_c\mathcal{C}. \end{aligned} \quad (24)$$

Under standard assumptions of stabilizability of  $(\mathcal{A}, \mathcal{B})$  and detectability of  $(\mathcal{A}, \mathcal{C})$ , there are guaranteed unique solutions

$\Pi$  and  $P$  to (15) and (23), respectively, such that the linear closed loop system given by

$$\frac{d}{dt} \begin{bmatrix} x(t) \\ x_c(t) \end{bmatrix} = \begin{bmatrix} \mathcal{A} & -\mathcal{BK} \\ \mathcal{F}_c \mathcal{C} & \mathcal{A}_c \end{bmatrix} \begin{bmatrix} x(t) \\ x_c(t) \end{bmatrix} + \begin{bmatrix} z - u_{fw} \\ \mathcal{F}_c v \end{bmatrix} \quad (25)$$

is stable.

The operators  $\mathcal{K}$ ,  $\mathcal{F}_c$ ,  $\mathcal{A}_c$  as determined above for the linearized system, are substituted into the corresponding nonlinear system

$$\dot{x}_{nl}(t) = \mathcal{A}_{nl}x_{nl}(t) + \mathcal{B}u_{nl}(t) + \mathcal{F}_{nl}(x_{nl}(t)) + \mathcal{G} + w(t), \quad (26)$$

thus producing the nonlinear observer

$$\dot{x}_c(t) = \mathcal{A}_c x_c(t) + \mathcal{F}_c y(t) + \mathcal{F}_{nl}(x_c(t)), \quad (27)$$

with an appropriate initial condition. Then the nonlinear closed loop system takes on the form

$$\frac{d}{dt} \begin{bmatrix} x_{nl}(t) \\ x_c(t) \end{bmatrix} = \begin{bmatrix} \mathcal{A}_{nl} & -\mathcal{BK} \\ \mathcal{F}_c \mathcal{C} & \mathcal{A}_c \end{bmatrix} \begin{bmatrix} x_{nl}(t) \\ x_c(t) \end{bmatrix} + \begin{bmatrix} z - u_{fw} + \mathcal{F}_{nl}(x_{nl}(t)) + \mathcal{G} \\ \mathcal{F}_c v + \mathcal{F}_{nl}(x_c(t)) + \mathcal{G} \end{bmatrix}. \quad (28)$$

### III. MULTIPLE COMPONENT STRUCTURE

Two Euler-Bernoulli beams connected at a rigid mass are used to model a flexible wing MAV. Each beam represents a wing with the rigid mass at the center representing a fuselage. It is assumed that the material properties of both beams are uniform, identical, and composed of latex and carbon-graphite fiber with epoxy. A graphical representation of the system can be seen in Figure 1. The vehicle is assumed

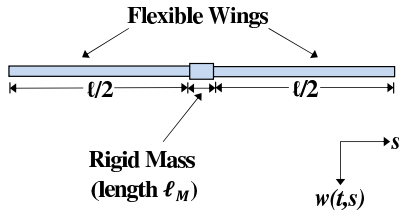


Fig. 1. MAV model system.

to be initially in flight, gliding with morphable wings as opposed to performing a flapping movement. (See [2] and [4] for projects on flapping flight.) Denoting the displacement (which is a combination of both rigid body and flexible motions) of the left beam from its initial equilibrium position at time  $t$  and position  $s_L$  by  $w_L(t, s_L)$  and the corresponding displacement of the right beam at time  $t$  and position  $s_R$  by  $w_R(t, s_R)$ , the model is described as follows:

$$\begin{aligned} & \rho A \ddot{w}_L(t, s_L) + \gamma_1 \dot{w}_L(t, s_L) \\ & + \gamma_2 I \dot{w}_L'''(t, s_L) + EI w_L''''(t, s_L) \\ & = b(s_L) u_L(t) + \frac{m_b g}{\ell_1} - \frac{0.5 \rho_a z^2 c}{\ell_1} C_\ell, \end{aligned} \quad (29)$$

for  $0 \leq s_L \leq \ell_1$ ,  $t > 0$ , and

$$\begin{aligned} & \rho A \ddot{w}_R(t, s_R) + \gamma_1 \dot{w}_R(t, s_R) \\ & + \gamma_2 I \dot{w}_R'''(t, s_R) + EI w_R''''(t, s_R) \\ & = b(s_R) u_R(t) + \frac{m_b g}{\ell_2} - \frac{0.5 \rho_a z^2 c}{\ell_2} C_\ell, \end{aligned} \quad (30)$$

for  $\ell_1 + \ell_M \leq s_R \leq \ell_1 + \ell_M + \ell_2$ ,  $t > 0$ . Here  $\dot{w}_i(t, s_i) = \frac{\partial}{\partial t} w_i(t, s_i)$  and  $w_i'(t, s_i) = \frac{\partial}{\partial s_i} w_i(t, s_i)$  with  $i = L, R$  for the left or right beam, respectively,  $\rho$  is the density of the beam material,  $A$  is the cross-sectional area of the beam,  $E$  is Young's modulus,  $I$  is the area moment of inertia of the beam,  $\gamma_1$  is the coefficient of viscous damping,  $\gamma_2$  is the coefficient of Kelvin-Voigt damping,  $g$  is gravity,  $m_b$  is the mass of each beam,  $b_L(s_L)$  is the control input function for the left beam,  $b_R(s_R)$  is the control input function for the right beam,  $u_L(t)$  is the controller for the left beam,  $u_R(t)$  is the controller for the right beam,  $\rho_a$  is the density of air,  $z$  is the forward vehicle velocity,  $c$  is the chord length of each wing (beam width), and  $C_\ell$  is the aerodynamic lift coefficient.

The aerodynamic lift coefficient applied to this model is the same one derived in [17] for a fruit fly model. While it was derived for a flapping flight insect, it should be noted that its relevance also holds in this framework due to the dimensionless property of the lift coefficient and the flexibility of the wings of the fruit fly. The lift coefficient model is scaled to the size of the MAV under consideration here by the parameters of the dynamic pressure,  $0.5 \rho_a z^2$ . Together the lift coefficient and the dynamic pressure make up the aerodynamic lift force,  $0.5 \rho_a z^2 c C_\ell$ . The lift coefficient is given by

$$C_\ell = \left[ k_1 + k_2 \sin \left( k_3 \arctan \left( \frac{\dot{w}(t, s) + k_5}{z} \right) + k_4 \right) \right], \quad (31)$$

where  $k_1, k_2, k_3, k_4$  are the best fit parameters determined from the analysis in [17]. In order to obtain real solutions and to accommodate atmospheric conditions, it has been assumed that  $k_4 = 0$ , and a new parameter,  $k_5$ , has been included in the model to reflect the vertical wind velocity.

The boundary conditions applied to these elastic equations arise from standard beam theory and are presented in (32).

$$\begin{aligned} & EI w_L''(t, 0) + \gamma_2 I \dot{w}_L''(t, 0) = 0, \\ & EI w_L'''(t, 0) + \gamma_2 I \dot{w}_L'''(t, 0) = 0, \\ & EI w_R''(t, \ell_1 + \ell_M + \ell_2) + \gamma_2 I \dot{w}_R''(t, \ell_1 + \ell_M + \ell_2) = 0, \\ & EI w_R'''(t, \ell_1 + \ell_M + \ell_2) + \gamma_2 I \dot{w}_R'''(t, \ell_1 + \ell_M + \ell_2) = 0, \\ & w_L(t, \ell_1) - w_R(t, \ell_1 + \ell_M) = 0, \\ & w_L'(t, \ell_1) - w_R'(t, \ell_1 + \ell_M) = 0, \\ & -EI w_L''(t, \ell_1) - \gamma_2 I \dot{w}_L''(t, \ell_1) + EI w_R''(t, \ell_1 + \ell_M) \\ & + \gamma_2 I \dot{w}_R''(t, \ell_1 + \ell_M) = I_z \ddot{w}_L'(t, \ell_1), \\ & EI w_L'''(t, \ell_1) + \gamma_2 I \dot{w}_L'''(t, \ell_1) - EI w_R'''(t, \ell_1 + \ell_M) \\ & - \gamma_2 I \dot{w}_R'''(t, \ell_1 + \ell_M) = m \ddot{w}_L(t, \ell_1). \end{aligned} \quad (32)$$

Employing a standard Galerkin finite element approximation (see [6] for details of the discretization), Equations (29) and

(30) can be written as a first order system of the form

$$\dot{x}(t) = Ax(t) + Bu(t) + G + F(x), \quad (33)$$

where

$$A = \begin{bmatrix} 0 & I \\ -M^{-1}K & -M^{-1}D \end{bmatrix}, \quad B = \begin{bmatrix} 0 \\ M^{-1}\bar{B} \end{bmatrix},$$

$$G = \begin{bmatrix} 0 \\ M^{-1}\bar{G} \end{bmatrix}, \quad F = \begin{bmatrix} 0 \\ M^{-1}\bar{F}(x) \end{bmatrix} \quad (34)$$

Here,  $x(t)$  represents the state of the system,  $M$ ,  $K$ , and  $D$  are the corresponding mass, stiffness, and damping matrices,  $\bar{B}$  is the control matrix,  $\bar{G}$  contains the gravity dynamics, and  $\bar{F}(x)$  contains the aerodynamic lift function.

#### IV. NUMERICAL RESULTS

For reference, the uncontrolled state plots for position and slope of the nonlinear system are given in Figure 2.

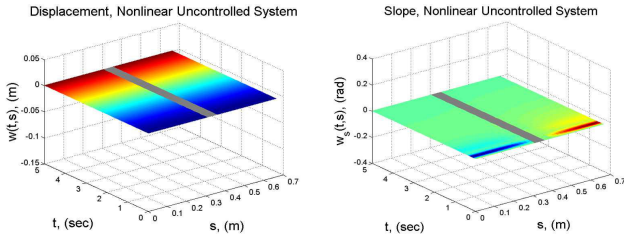


Fig. 2. Uncontrolled System: Position (left), Slope (right)

##### A. Feedback Linearization Results

Equations (33) and (34) are then employed for performing a feedback linearization on the beam-mass-beam system. Note that while (33) is nonlinear in the states, it is an input-affine system. Treating the output of the system to be the displacement and slope along the length of the beam and the input to be provided by actuators that are distributed throughout the length of the beam, (33) and (34) form a square system (that has an equal number of inputs and outputs). Since the input at each point directly influences the second derivative of the output at that point, each such output has a relative degree of two. Furthermore, it can be seen that the discretized system has total relative degree equal to the number of states, which implies that the system has no internal dynamics [18]. Thus, input-output linearization as well as input-state linearization can be simultaneously achieved for the beam-mass-beam system.

Once the system has been feedback-linearized, we then construct an outer-loop that comprises a sliding mode controller, as discussed in an earlier section of this paper. The desired morphing trajectory is depicted in Figure 3. A convergent finite element approximation using Hermite interpolating cubic polynomials of order  $N = 15$  nodes for the spatial discretization of the BMB system is used to simulate (33), and the parameter values for the BMB system are provided in Table I. Figure 4 shows the ensuing morphing trajectory, while Figure 5 demonstrates the control effort.

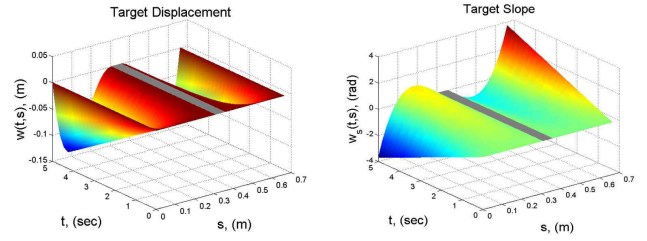


Fig. 3. Desired State Target: Position (left), Slope (right)

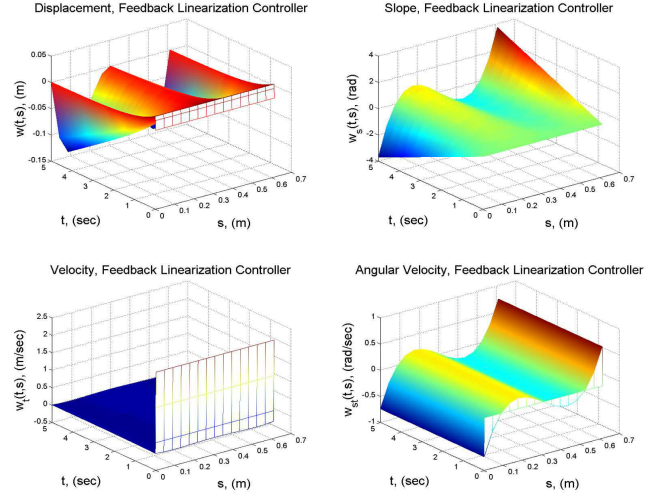


Fig. 4. Feedback-linearized system: Position (Top Left), Slope (Top Right), Velocity (Top Left), Angular Velocity (Top Right)

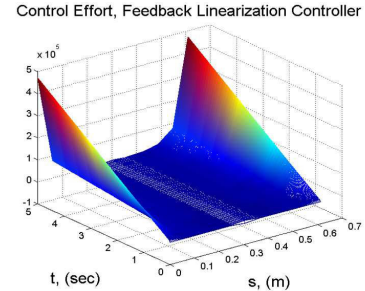


Fig. 5. Feedback-linearized system: Control Effort

##### B. Linear Quadratic Tracking Results

Before designing control for the system, we first obtain a linear approximation for (29) and (30). The type of linearization employed here is motivated by the fact that the system sees two zero eigenvalues due to the free end conditions for displacement and slope. In order to make the  $A$  matrix from (33) aware of a weight force in the system,  $m_b g$  is approximated by the following

$$m_b g \approx m_b \ddot{w}(t, s). \quad (35)$$

Further, to provide the  $A$  matrix with knowledge of the aerodynamic lift force, a linear approximation of  $C_l$  is calculated using a Taylor series expansion about a zero angle

of attack. Therefore for small angles of attack, the following approximation is reasonable and applied here:

$$\arctan\left(\frac{\dot{w}(t,s) + k_5}{z}\right) \approx \frac{\dot{w}(t,s) + k_5}{z}. \quad (36)$$

Making this substitution into (31), applying a Taylor expansion, and keeping only the linear term yields the following:

$$C_l \approx \frac{k_2 k_3}{z} \dot{w}(t,s). \quad (37)$$

We then apply these substitutions to (29) and (30) and obtain a Galerkin finite element approximation for the linearized system, upon which control design is employed. The appropriate control matrices are then applied to the nonlinear system. Since one goal of this project is to gain insight into optimal morphing trajectory, it is assumed that the controllers act over the entire beam structure with constant control input functions of the form

$$b(s_L) = b(s_R) = 1000, \quad (38)$$

for  $0 \leq s_L \leq \ell_1$  and  $\ell_1 + \ell_M \leq s_R \leq \ell_1 + \ell_M + \ell_2$ , and observations of the form

$$y(t) = 650w(t,s), \quad (39)$$

for  $0 \leq s_L \leq \ell_1$  and  $\ell_1 + \ell_M \leq s_R \leq \ell_1 + \ell_M + \ell_2$ . The magnitudes of the two functions in (38) and (39) were chosen in order to alleviate overshoot in the LQG-controlled system. However, it should be noted that controller multipliers chosen two orders of magnitude less and measurement multipliers chosen one order of magnitude less produce good results for the LQR-controlled system, but some oscillatory behavior in the LQG-controlled system.

Since this control approach specifies a trajectory for all four states ([position; slope; velocity; angular velocity]), we take initial conditions to be of the form:  $x(0) = [0; 0; 0; 0]$ . For the coupled state and state estimate system, the initial condition  $x_c(0) = 0.75 * x(0)$  is used. It should also be noted that the balancing lift and weight forces are modeled in the state estimate system as well. A convergent finite element approximation using Hermite interpolating cubic polynomials of order  $N = 31$  nodes for the spatial discretization of the BMB system is used to simulate (33), and the parameter values for the BMB system are provided in Table I. Controlled results are presented in Figures 6 and 7, excluding noise. The corresponding controller plots are shown in Figure 8. To obtain stabilizing solutions to the algebraic Riccati equations, a Newton-Kleinman algorithm was used. For the results presented here, it is assumed that measurements are available for the position and slope states.

## V. CONCLUSIONS AND FUTURE WORKS

### A. Conclusions

This work has considered a multiple component structure consisting of two Euler-Bernoulli beams connected to a rigid mass, used to model the heave dynamics of an aeroelastic wing micro air vehicle. The vehicle is assumed to be acted upon by a nonlinear aerodynamic lift force. We have

TABLE I  
SYSTEM PARAMETERS

Parameter	Value	Units
$\ell_{1,2}$	0.6096	m
$\ell_M$	0.0508	m
$\rho$	980	kg/m <sup>3</sup>
$\hat{w}$ , width	0.127	m
$h$ , height	0.0254	m
$a = \hat{w}h$	0.032	m <sup>2</sup>
$E$	$2.0 \times 10^6$	N/m <sup>2</sup>
$I = (\hat{w}h^3)/12$	$1.734 \times 10^{-7}$	m <sup>4</sup>
$m$	1.927	kg
$m_b$	1.927	kg
$\gamma_1$	0.025	kg/(m sec)
$\gamma_2$	$1 \times 10^2$	kg/(m <sup>5</sup> sec)

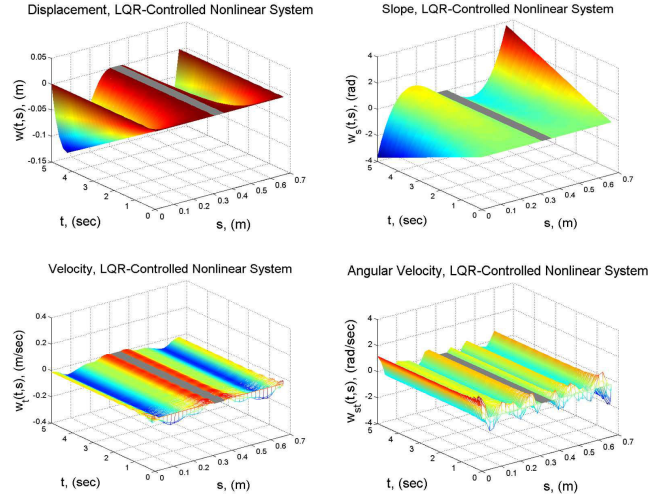


Fig. 6. Controlled System: LQR Position (top left), LQR Slope (top right), LQR Velocity (bottom left), LQR Angular Velocity (bottom right)

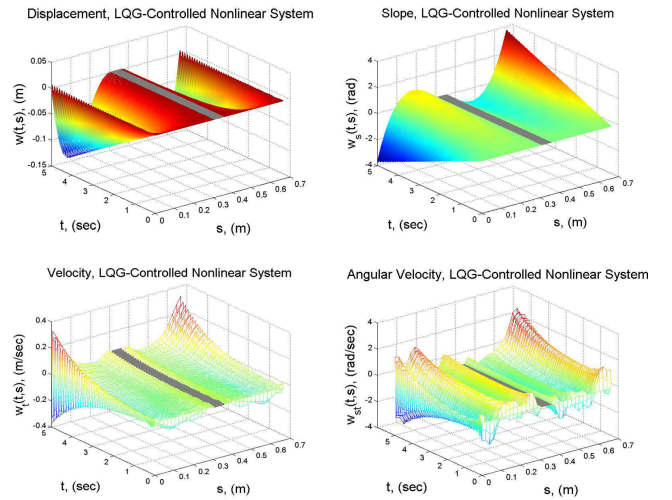


Fig. 7. Controlled System: LQG Position (top left), LQG Slope (top right), LQG Velocity (bottom left), LQG Angular Velocity (bottom right)

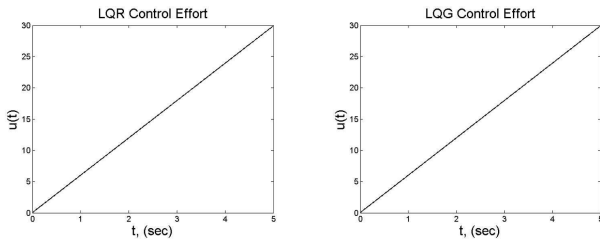


Fig. 8. Control Effort: LQG (left), LQR (right)

examined two different strategies for designing nonlinear controllers that achieve specified wing morphing trajectories, namely (a) linearization followed by linear quadratic tracking and (b) a feedback linearization inner loop with sliding mode outer loop.

With regard to the controllers designed using the feedback linearization and linear quadratic strategies, we see that they perform well and each system is able to morph to the desired position and slope along the specified trajectory. The closed loop state responses (those that are tracked) are quite similar to each other, yet the control inputs of the linear quadratic strategy are considerably different from those in the feedback linearization strategy. This is likely to be expected for the following reasons.

- 1) In LQR, the control across the whole BMB system is scaled by a pre-defined constant and thus the BMB is essentially modeled as a single input system, even though the control is distributed, whereas in feedback linearization the BMB is modeled as a true multiple input multiple output (MIMO) system.
- 2) In LQR, the goal of the control is purely one of tracking, whereas in feedback linearization the goal of the control is both of canceling the nonlinearities in the system as well as tracking. The feedback linearization might thus be “over-reaching” in that in its goal to make the closed loop linear, it might even be canceling some “good” nonlinearities.

We see that both the LQR and LQG tracking perform quite comparably except for the velocity and angular velocity states, likely since we did not measure those states in the LQG design, where we actually see growth in the velocity and angular velocity near the free ends of the beams. The unreasonably and unrealistically large angular velocity found in the LQG controlled system is roughly twice the magnitude of the angular velocity found in the LQR and feedback linearized systems, and it does present a severe limitation in the LQG compensator-based approach for control design on this problem.

### B. Future Work

Future work includes investigating optimal morphing trajectories and applying realistic actuation to the model. Results with piezoceramic patch actuators attached to the beams will be the subject of another paper. Theoretical analysis, including model well-posedness and semigroup results, are forthcoming in a separate paper as well.

## VI. ACKNOWLEDGMENTS

The authors gratefully acknowledge the contribution of the Louisiana Board of Regents, the US Air Force Summer Faculty Fellowship Program, the Air Force Research Laboratory and reviewers’ comments. Portions of this research were conducted with high performance computational resources provided by the Louisiana Optical Network Initiative (<http://www.loni.org/>).

## REFERENCES

- [1] W. Shyy, P. Ifju, and D. Vieru, “Membrane wing-based micro air vehicles,” *Applied Mechanics Reviews*, vol. 58, pp. 283–301, 2005.
- [2] W. Shyy, P. Trizila, C. Kang, and H. Aono, “Can tip vortices enhance lift of a flapping wing?” *AIAA Journal*, vol. 47, pp. 289–293, 2009.
- [3] X. Tian, J. Iriarte-Diaz, K. Middleton, R. Galvao, E. Israeli, A. Roemer, A. Sullivan, A. Song, S. Swartz, and K. Breuer, “Direct measurements of the kinematics and dynamics of bat flight,” *Bioinspiration & Biomimetics*, vol. 1, pp. S10–S18, 2006.
- [4] A. Song, X. Tian, E. Israeli, R. Galvao, K. Bishop, S. Swartz, and K. Breuer, “Aeromechanics of membrane wings, with implications for animal flight,” *AIAA Journal*, vol. 46, no. 8, pp. 2096–2196, 2008.
- [5] A. Chakravarthy, K. Evans, and J. Evers, “Sensitivities and functional gains for a flexible aircraft-inspired model,” *Proceedings of the 2010 American Control Conference*, pp. 4893–4898, 2010.
- [6] A. Chakravarthy, K. Evans, J. Evers, and L. Kuhn, “Target tracking strategies for a nonlinear, flexible aircraft-inspired model,” *Proceedings of the 2011 American Control Conference*, to appear.
- [7] P. D. Christofides, *Nonlinear and Robust Control of PDE Systems*. Boston, MA: Birkhäuser, 2001.
- [8] A. Balogh and M. Krstic, “Infinite dimensional backstepping-style feedback transformations for a heat equation with an arbitrary level of instability,” *European Journal of Control*, vol. 8, no. 2, pp. 165–175, 2002.
- [9] M. Krstic, A. Smyshlyaev, and R. Vazquez, “Infinite-dimensional backstepping and applications to flows in electromagnetic fields,” *Proceedings of the 16th Mediterranean Conference on Control and Automation*, pp. 1–14, 2008.
- [10] M. Krstic and A. Smyshlyaev, *Boundary Control of PDEs: A Course on Backstepping Designs*. Philadelphia: SIAM, 2008.
- [11] S. A. Wadoo, “Evacuation distributed feedback control and abstraction,” Ph.D. dissertation, Virginia Polytechnic Institute and State University, April 2007.
- [12] S. A. Wadoo and P. Kachroo, “Feedback control of crowd evacuation in one dimension,” *IEEE Transactions on Intelligent Transportation Systems*, vol. 11, no. 1, pp. 182–193, 2010.
- [13] B. Fernandez and J. K. Hedrick, “Control of multivariable nonlinear systems by the sliding mode method,” *International Journal of Control*, vol. 46, no. 3, pp. 1019–1040, 1987.
- [14] J. S. Gibson, “An analysis of optimal model regulation: convergence and stability,” *SIAM J. Contr. Opt.*, vol. 19, pp. 686–707, 1981.
- [15] J. S. Gibson and A. Adamian, “Approximation theory for linear quadratic gaussian control of flexible structures,” *SIAM J. Contr. Opt.*, vol. 29, pp. 1–37, 1991.
- [16] P. Dorato, C. Abdallah, and V. Cerone, *Linear-Quadratic Control, An Introduction*. Englewood Cliffs: Prentice Hall, 1995.
- [17] M. Dickinson, F. Lehmann, and S. Sane, “Wing rotation and the aerodynamic basis of insect flight,” *Science*, pp. 1954–1960, June 1999.
- [18] J.-J. E. Slotine and W. Li, *Applied Nonlinear Control*. Englewood Cliffs, New Jersey: Prentice Hall, 1991.